



UV-assisted photo-catalytic degradation of anionic dye (Congo red) using biosynthesized silver nanoparticles: a green catalysis

Wasim Akram Shaikh^a, Sukalyan Chakraborty^{a,*}, Rafique Ul Islam^b

^aEnvironmental Engineering Laboratory, Department of Civil & Environmental Engineering, Birla Institute of Technology, Mesra 835215, India, emails: su_kalyanc@yahoo.co.uk, sukalyanchakraborty@bitmesra.ac.in (S. Chakraborty), wasim.bu12@gmail.com (W.A. Shaikh)

^bDepartment of Chemistry, School of Physical and Material Sciences, Mahatma Gandhi Central University, Motihari, Bihar 845401, India, email: rafique@mgcub.ac.in

Received 20 March 2018; Accepted 18 August 2018

ABSTRACT

Congo red (CR) is an anionic synthetic dye used in many industrial and scientific applications, has considerable toxic effects when released into the ecosystems without treatment. This study is focussed on its degradation using silver nanoparticles (AgNPs) synthesized from silver nitrate using *Azadirachta indica* leaf extract. The synthesized green colloidal AgNPs were validated and characterized by UV–vis spectra, transmission electron microscopy (TEM), energy dispersive X-ray (EDX) and X-ray diffraction (XRD) analysis. Specific interactions during bioreduction process and biomolecules responsible for capping, reducing and stabilizing were determined by Fourier transform infrared spectroscopy analysis. TEM image confirmed the size of the spherical AgNPs ranging between 11 and 35 nm. EDX and XRD analysis confirmed the metallic form of the synthesized AgNPs, while selected area electron diffraction pattern revealed its crystalline nature. The biosynthesized AgNPs were found to be very effective for the photo-catalytic degradation of toxic industrial anionic dye, CR under UV source. Further optimization of the process variables viz. effect of initial dye concentration, UV irradiation time, catalyst dose, temperature and pH showed significant degradation up to 90% following pseudo-first-order kinetic model. Degraded dye was tested for toxicity by germination test of Bengal Gram (*Cicer arietinum*), which indicated no toxicity. Hence it can be concluded that the current method of synthesis has the potentiality to form stable AgNPs, which can have promising application potential for dye removal in environment management.

Keywords: Silver nanoparticle; Green synthesis; Photo-catalytic degradation; Congo red; Degradation kinetics; Mechanism

1. Introduction

Synthetic dyes used in textile, paper, plastic, cosmetic, leather, food and pharmaceutical industries have several deleterious effect on environment and life cycle of aquatic organisms due to their high degree of toxicity [1]. The estimated numbers of commercially available dyes are more than 100,000, and among them over 10,000 type of dyes are used routinely in industries, resulting in 0.7 million tons

dyestuff produced as effluents per annum [2]. Some of these dyes were even identified as potential carcinogens [3].

Several conventional techniques have been applied extensively for the mitigation of these dyes such as membrane filtration, enhanced ultrafiltration, coagulation/flocculation, electrochemical process, adsorption on activated carbon, reverse osmosis, chemical oxidation, electrocoagulation, electrodialysis and chemical precipitation [4,5]. Recently some advanced treatment technologies such as integrated chemical–biological degradation, solar photo-Fenton method, Fenton-biological treatment method, sonochemical degradation, cation exchange membranes and photo-assisted

* Corresponding author.

biological treatment have also been used to decolourize these synthetic dyes and overcome the limitations of traditional methods [6,7]. However, all of these methods exhibited some disadvantages, such as use of toxic chemicals, requirement of huge amount of chemical and/or adsorbent, costly running process, use of expensive equipment and selective operating conditions with less efficiency [8]. In the existing scenario nanomaterials brought great opportunities in dye degradation from wastewater. A wide range of nanomaterials such as TiO_2 , metal oxides, graphene oxide, nanochitosan, carbon nanotubes, metal hexacyanoferrate nanoparticles (NPs) and MoS_2 nanosheets have been used for dye removal [9–11]. Among the different metallic NPs, especially silver nanoparticles (AgNPs) have gained immense importance owing to their electrical, thermal and optical properties [12]. Due to high surface area as well as the catalytic activity, AgNPs have emerged as a potent reducer of synthetic dyes [13].

Some of the conventional techniques for synthesis of the mentioned nanomaterials have been reduction in solutions, chemical and photochemical reactions, ion sputtering, sol-gel, autoclaving, electrochemical, gamma ray radiation and microwave-assisted process [14]. However, all these methods posed their own limitations, such as requirement of capping agent in chemical methods to prevent agglomeration, which is generally toxic in nature, need for high vacuum technology and expensive equipments in physical methods. Even nonpolar solvents and presence of toxic chemicals on surface became a hindrance for their applications in several fields [15]. Therefore, recently NP synthesis method is focussed towards biological or green pathways. Green synthesis of NPs is the emerging branch of nanotechnology which utilizes benign materials such as plant extract [12], bacteria [16] and fungi for synthesis of nanomaterials [17]. These green bioreduction processes have been found to be successfully producing cost-effective, environment-friendly and nontoxic metallic NPs [10]. It was also observed that among the various conventional and advanced technologies, biosynthesized NPs drew tremendous attention as a photo-catalyst due to presence of surface plasmon resonance (SPR) phenomenon [18], large surface area, good conductivity [19], chemical stability [10] and most importantly being nontoxic in nature [12].

Biosynthesized AgNPs using various biological extracts, that is, *Hypnea musciformis*, a red algae, *Saccharomyces cerevisiae* extract, *Trigonella foenum-graecum* seeds and *Artemisia tournefortiana* aerial part extract have been found to be very effective in degrading methyl orange [20], methylene blue [21], eosin Y [22] and Coomassie Brilliant Blue G-250 [23], respectively. Considering the above facts, this study was attempted to degrade a synthetic anionic dye, Congo red (CR) through photo-catalytic degradation with the help of biosynthesized AgNPs. CR, an anionic acid dye used in laboratory for amyloidosis diagnosis, histological stain for amyloid and a pH indicator. CR, a potent toxic dye, shows ameliorative effect which causes neurodegenerative disorders, such as Alzheimer's, Huntington's, Parkinson's and prion diseases [24]. It is also reported that CR is a potent mutagen which causes reproductive effect, gastrointestinal irritation, respiratory problems, affects blood clotting, can reduce the concentration of serum protein, disseminated micro-embolism, causes platelet aggregation, arrests cell division and

induces somnolence [24,25]. In addition, experiments have revealed CR as teratogen and two CR derivatives (benzidine and naphthoic acid) to be co-carcinogen.

Biosynthesis of AgNPs was executed with neem leaf extract (*Azadirachta indica*). Neem or Indian Lilac belongs to the Meliaceae family. It is a fast-growing, evergreen tree, which is native of Indian subcontinent typically grown in tropical and semitropical regions. Wide ranges of biochemicals such as alkaloids, carbohydrates, reducing sugar, flavonoids, glycosides, hydroxypivalic acid ($\text{C}_5\text{H}_{10}\text{O}_3$), phytol ($\text{C}_{20}\text{H}_{40}\text{O}$) and germanicol ($\text{C}_{30}\text{H}_{50}\text{O}$) were reported to be found in *A. indica* leaf extract that may act as reducing as well as capping agent during the synthesis of AgNPs in the green process [26]. Further optimization of the reaction variables were carried out for obtaining the best performance of degradation.

2. Materials and methods

2.1. Chemicals and plant material collection

All the chemicals and reagents including silver nitrate (AgNO_3) used were of Merck empla grade and used without further purification. Fresh leaves of *A. indica* were harvested from BIT campus, Ranchi, Jharkhand, India. All the aqueous solutions for this investigation were prepared using Milli-Q water.

2.2. Preparation of plant extract

For bioreduction of AgNPs, fresh leaves of *A. indica* were collected and washed thoroughly using tap water to clean its surface to remove the debris, other organic contents and adhered impurities. Then the leaves were rinsed thrice with double distilled water and air dried at room temperature in shade to remove moisture. After that 25 g of freshly washed green leaves was crushed with Milli-Q water and final volume made up to 100 mL. This method of extraction was slightly modified from the method of Ref. [27], who carried out the extraction by boiling the neem leaves. The solution containing crushed leaves was then centrifuged for 10 min at 13,000 rpm and the supernatant was filtered using Whatman filter paper No. 1 and the extract was stored at 4°C for further use.

2.3. Biosynthesis of AgNPs

Silver nitrate working solutions (1, 2, 3 and 4 mM) were prepared with Milli-Q water and 1 mL aliquot of leaf extract was added to each working solution (25 mL) in Erlenmeyer flasks, covered with aluminium foil and continuously stirred in room temperature in dark condition for bioreduction. The appearance of brownish yellow colour of colloidal solution confirmed the reduction and formation of AgNPs. Optimization of AgNO_3 concentration for best reduction was done based on colour and spectral analysis using Shimadzu UV-visible spectrophotometer (Model: UV-1800) with a range of 200–800 nm. Then the process was repeated varying the leaf extract to standardize its volume by adding 1, 2, 3 and 4 mL of leaf extract into the optimum strength AgNO_3 solution. To optimize the reduction time, the experiment was performed up to 120 min with a periodic interval of 15 min

in optimized condition. The colloidal solutions were kept for further characterization after removing water soluble biomolecules by repeated centrifugation using Milli-Q water.

2.4. Characterization of synthesized AgNPs

The morphology, particle size and elemental composition of the AgNPs were analyzed by using transmission electron microscopy (TEM) and electron dispersive X-ray (Jeol, Japan, JSM-6390 LV). TEM was done using Phillips TEM (CM 200; Operating Voltage: 20–200 kV, Resolution: 2.4 Å) on copper-coated carbon grid. The crystalline structure and phase of the AgNPs were determined by X-ray diffraction (XRD) technique using Bruker D8 advanced X-ray diffractometer with Bragg-Brentano goniometer geometry and Cu-K α X-radiation ($\lambda = 1.5418$ Å). To identify the functional groups of associated biomolecules in leaf extract, Fourier transform infrared spectroscopy (FTIR) spectra of AgNPs was studied using Shimadzu Corporation, Japan, IR-Prestige 21.

2.5 Photo-catalytic Degradation

The photo-catalytic activity of synthesized AgNPs was evaluated by the degradation of CR in aqueous solution in the presence of UV irradiation in a photo-catalytic chamber. Initially, 4 mL colloidal AgNPs was mixed with 30 mL of CR solution (20 mg/L) (1:7.5 ratio) in a 250 mL conical flask under UV light irradiation (using 11 W UV light) and stirred constantly for about 120 min to allow the degradation reaction. Samples were collected in periodic intervals (in every 15 min) and centrifuged at 10,000 rpm for 5 min. After centrifugation, the absorption spectrum of the aliquots was analysed between 200 and 800 nm using a UV-visible spectrophotometer and to estimate the photo-catalytic efficiency the characteristic peak was monitored at 500 nm. To determine the catalytic activity or physical adsorption onto the surface of AgNPs, one setup was carried out with the same condition (1:7.5 ratio) in dark. Another control was performed in the presence of UV light without AgNPs. pH of the CR solutions was adjusted using 0.1 M hydrochloric acid (HCl) or sodium hydroxide (NaOH) to determine the effect of pH on the photo-catalytic efficiency according to the experiment of Ref. [28]. Finally, the percentage of photo-catalytic efficiency (%) was calculated by the following formula [29]:

$$\text{Photo-catalytic efficiency (\%)} = \frac{C_o - C_t}{C_o} \times 100 \quad (1)$$

where C_o is the initial concentration of CR solution, C_t is the concentration of CR solution at the irradiation time (t). The photo-catalytic degradation of CR was optimized by optimizing various parameters such as irradiation time (00–120 min), initial dye concentration (1–30 mg/L), dose (1:1–1:10 ratio), temperature (283–323 K) and pH (pH 2–10).

2.6. Seed germination test

The toxicity of the degraded product of CR was determined by germination test of Bengal Gram (*Cicer arietinum*) seeds. Bengal Gram is commonly known as chickpea, a

legume, which belongs to the Fabaceae family, subfamily Faboideae. The seeds were subjected to two different concentrations of CR dye (10 and 20 mg/L) and degraded product for 5 d, keeping one set of control with only double distilled water. On the fifth day, observations were recorded and degree of toxicity was calculated, based on germination percentage and seedling vigour index.

Germination percentage was determined by the following formula:

$$\text{Germination percentage} = \frac{\text{No. of seed germinated}}{\text{Total No. of seeds}} \times 100 \quad (2)$$

Seedling Vigour Index was calculated as follows:

$$\text{SVI} = (\text{Seedling length (cm)} \times \text{Germination percentage}) \quad (3)$$

3. Results and discussions

3.1. Biosynthesis of AgNPs

The colour of the silver nitrate solution changed from colourless to brownish yellow after addition of *A. indica* leaf extract indicating the bioreduction process [15]. This normally happens due to surface plasmonic resonance (SPR) caused by combined oscillation of free conduction electrons, prompted by an interacting electromagnetic field [30]. Fig. 1(a) shows the variation in colour between AgNO₃ solution, leaf extract and colloidal AgNPs. When the silver nitrate solution was treated with varying amounts of leaf extracts, viz., 1, 2, 3 and 4 mL, characteristic colour gradient due to SPR variation could be observed in each, increasing with volume of leaf extract represented in Fig. 1(b). UV-vis spectrum analysis further confirmed the bioreduction of AgNO₃ to metallic AgNPs by their optical properties. Maximum absorption in UV-vis spectra was observed for the solution with 3 mL of leaf extract indicating maximum formation of AgNPs. Formation of AgNPs with respect to duration of reaction (15–120 min) showed increasing peaks with increase in time up to 120 min of the experiment (Fig. 1(c)). Ref. [31] has reported similar observation with *Adenium obesum* leaf extract, where the absorbance peaks became sharper and colour of the colloidal solution became nearly constant, indicating the saturation of silver salt in the solution after 120 min. The result also suggested the synthesis rate of AgNPs to be directly proportional to the incubation period.

3.2. Characterization of the synthesized AgNPs

TEM, which is one of the best tools to determine structural, morphological properties and size distribution [32] elucidated well dispersed and spherical AgNPs with particle size ranging between 11 and 35 nm (Figs. 2(a) and (b)). SAED patterns of the biosynthesized AgNPs showed prominent diffraction rings and spots, suggesting crystalline structure of silver according to the JCPDS cards (JCPDS ID: 01-087-0719) with their respective TEM image. Fig. 2(c) presents prominent diffraction rings and spots, clearly indicating crystallinity of AgNPs. The pattern formed towards the core of the rings was also stable with the d-spacing and matched with the fcc phase of AgNPs as investigated through XRD [18].

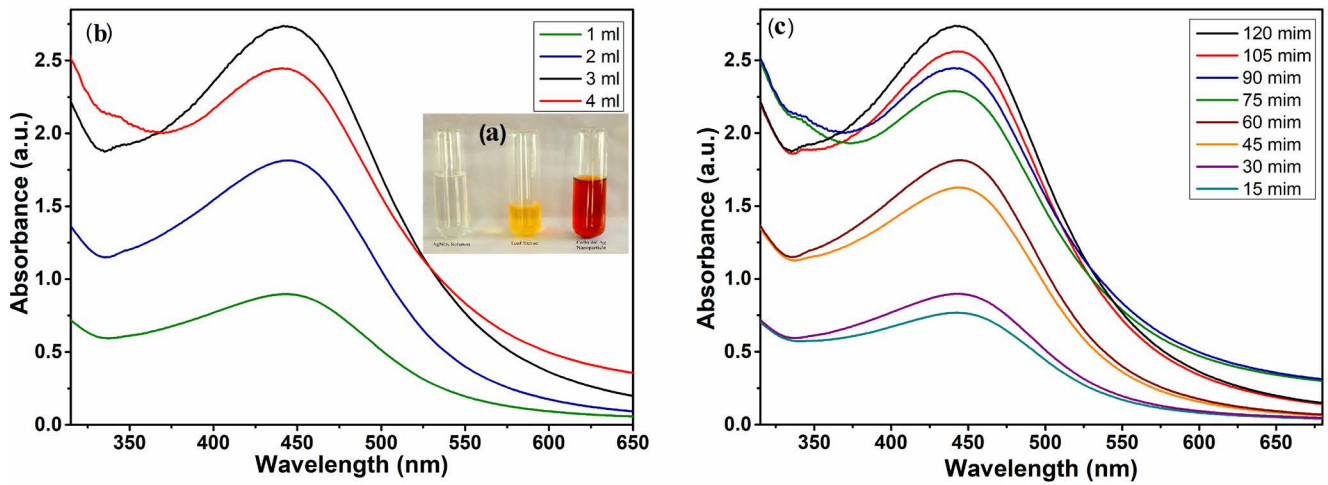


Fig. 1. (a) (inset) AgNO_3 , leaf extract and synthesized colloidal silver nanoparticles, (b) UV–visible spectrum of synthesized AgNPs at different quantities of *A. indica* leaf extract and (c) UV–visible spectrum of silver nanoparticles synthesized at different time intervals.

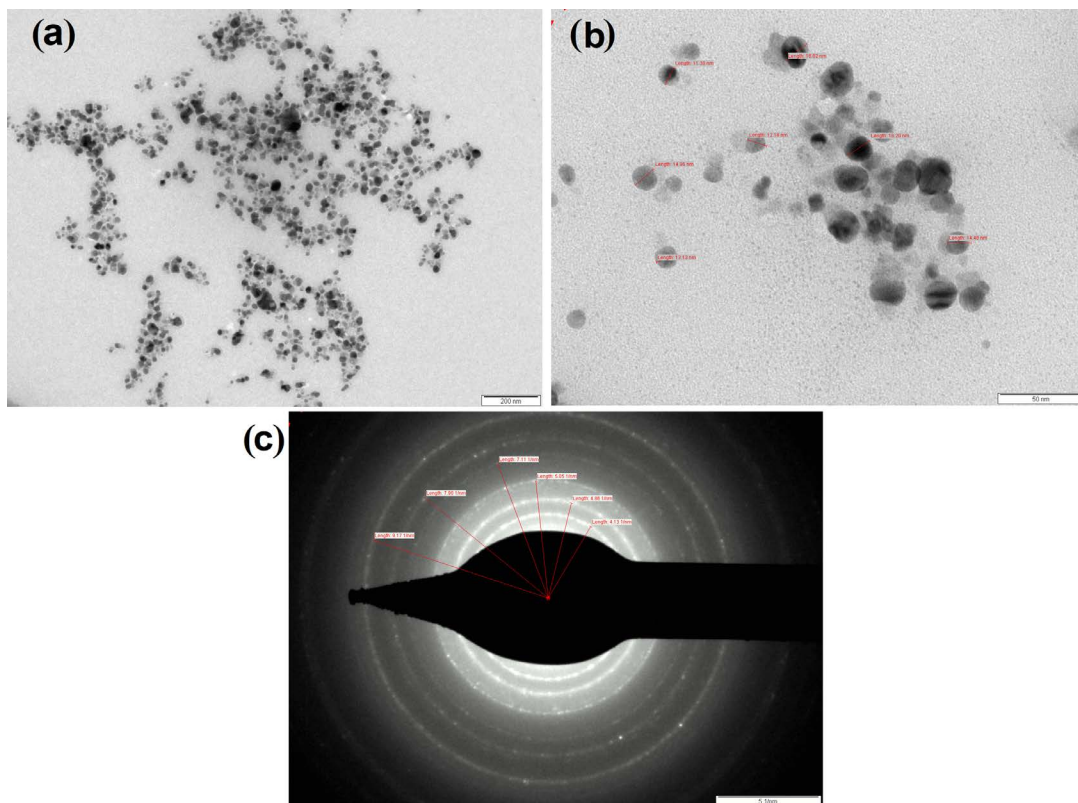


Fig. 2. TEM image of AgNPs (a) 200 nm, (b) 50 nm scale bar and (c) selected area electron diffraction ring (SAED) patterns of the synthesized AgNPs.

The XRD analysis of the colloidal AgNPs confirmed their nanocrystalline nature, as evidenced by the peaks at 2θ values of 38.1° , 44.3° , 64.4° and 77.4° corresponding to (111), (231), (220) and (311), respectively Bragg reflections of silver (Fig. 3) [33]. The XRD results clearly showed that the AgNPs formed were crystalline in nature. The nanocrystalline nature of the AgNPs is in good agreement with the TEM studies and literature reported for green synthesis of AgNPs [34].

The elemental composition of the formed AgNPs by energy dispersive X-ray (EDX) showed characteristic prominent silver peak in EDX image (Fig. 4(a)) suggesting the presence of Ag as the major element (Weight % 75.51; Atomic % 29.45). Some low intense peaks of Ca, C, and O also coexisted with the high intense peak. This might be due to the presence of capping biomolecules of *A. indica* leaf extract on the surface of the AgNPs in Fig. 4(b) [35].

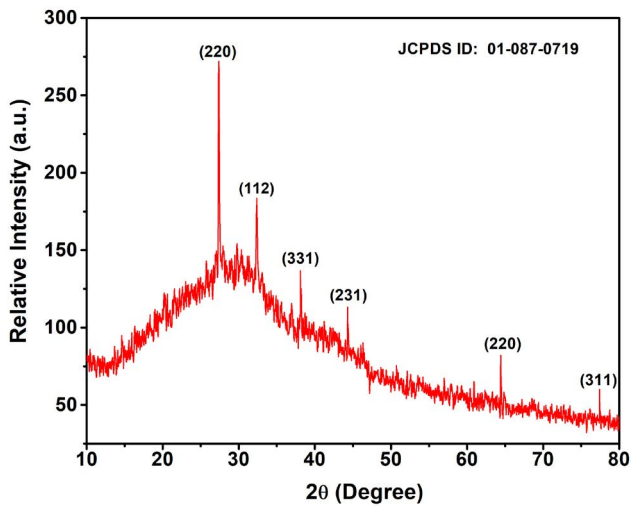


Fig. 3. XRD spectrum of biosynthesized AgNPs.

FTIR spectrum of colloidal AgNPs was investigated between the wavenumber 4,000 and 400 cm^{-1} . Peak between 2,800 and 3,500 cm^{-1} recognized hydroxyl ($-\text{OH}$) of phenolic compound, peak at 2,063 cm^{-1} indicated presence of alkynes group. After synthesis, peak of amide shifted to 1,678 cm^{-1} from 1,650 cm^{-1} , which might be due to the presence of leaf extract proteins [36]. Some weak aromatic $-\text{CH}$ peaks have also been observed between 920 and 780 cm^{-1} [37] (Fig. 5).

3.3. Photo-catalytic degradation

Experiment performed in presence of AgNPs under UV illumination, showed rapid deformation and decrease in intensity of absorption peaks at 500 nm indicating photo-catalytic degradation of CR [38]. FTIR spectra of the degraded dye showed prominent changes in the functional groups after degradation with respect to the initial one (Fig. 6). Major peaks at 3,468 cm^{-1} for alcohol/phenol O–H stretch, 1,589 cm^{-1} for aromatic C=C bending, 1,357 cm^{-1} for aromatic N–O bond, 1,226 cm^{-1} for C–O stretch, 1,186 cm^{-1} for C=O

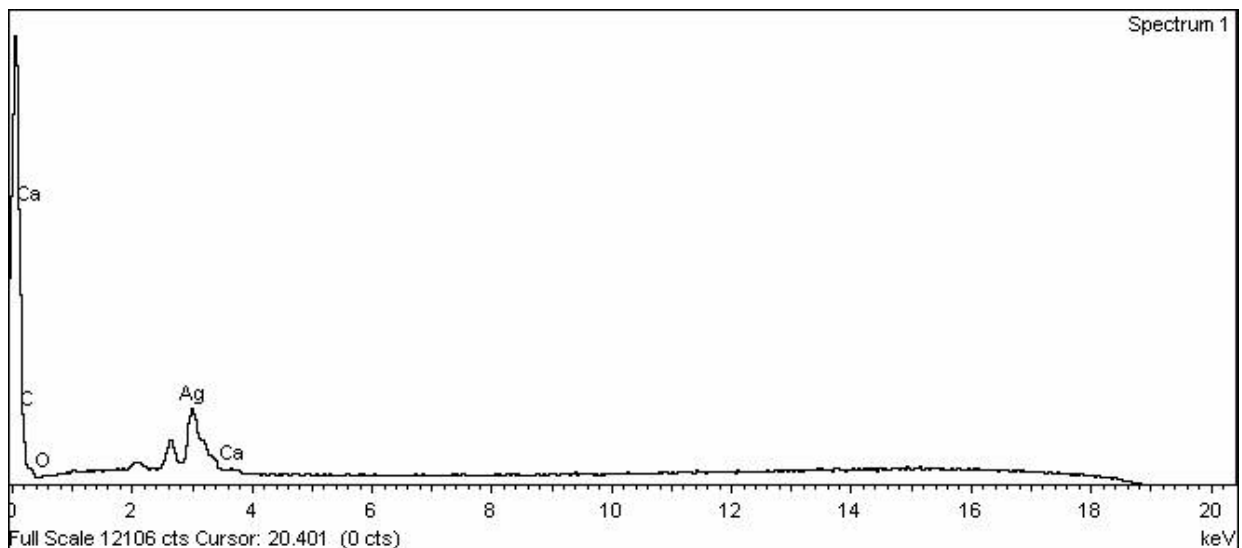
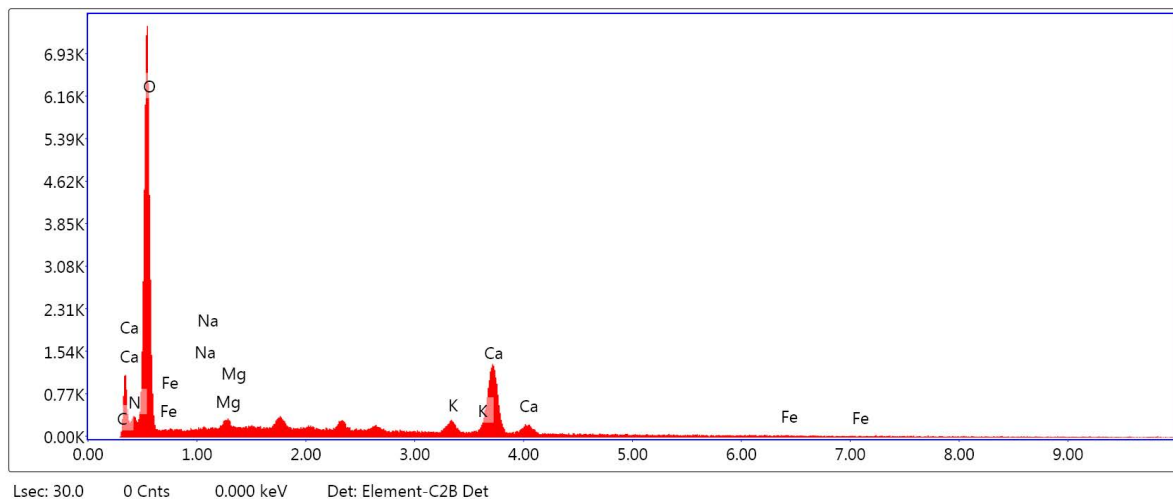


Fig. 4(a) EDX pattern of synthesized AgNPs and (b) EDX pattern of *A. indica* leaf extract.



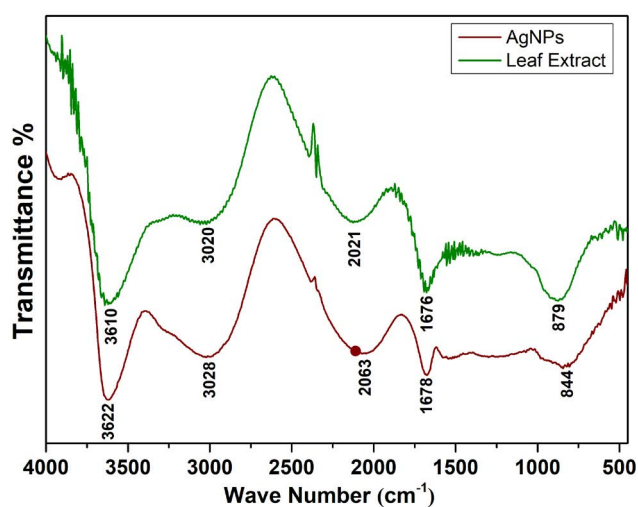


Fig. 5. FTIR spectrum of the *A. indica* leaf extract and metallic AgNPs.

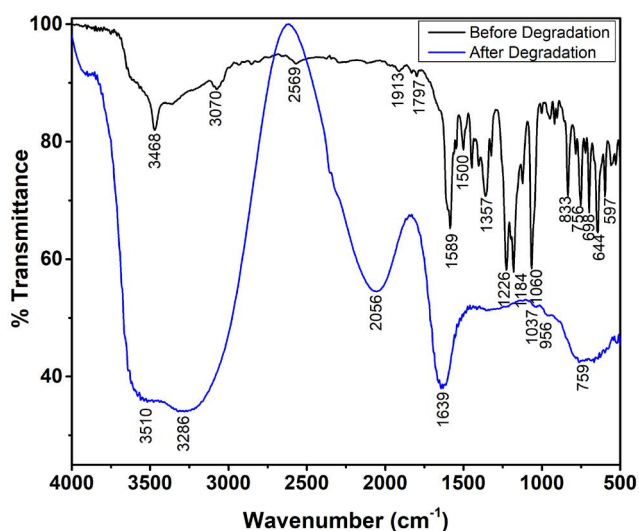


Fig. 6. FTIR spectrum before and after degradation of the Congo red dye.

stretch and $1,060\text{ cm}^{-1}$ for alcoholic C–O stretch and some weak peaks at $3,017\text{ cm}^{-1}$ for alkenyl C–H stretch, $2,569\text{ cm}^{-1}$ for carboxylic O–H stretch, $1,913\text{ cm}^{-1}$ for aromatic C–H bending, $1,797\text{ cm}^{-1}$ for C=O stretch, $1,500\text{ cm}^{-1}$ for aromatic C=C bending and 756 cm^{-1} for C–H bond were observed in the dye before degradation. While after degradation two major peaks at $2,056$ and $1,639\text{ cm}^{-1}$ corresponding to C=C=N stretching and alkenyl C=C stretch and low intense peaks at $3,510\text{ cm}^{-1}$ for amide N–H stretch, $1,037\text{ cm}^{-1}$ for CO–O–CO stretch, 956 cm^{-1} for C=C bending and 759 cm^{-1} for aromatic C–H bending were observed. A large hump at $3,286\text{ cm}^{-1}$ was also seen in degraded dye spectra of CR corresponding to alcohol/phenol O–H stretch. Disappearance of the significant peaks in degraded dye spectra can be due to breaking of dye molecule.

However, control experiment performed in UV irradiation without AgNPs showed neither shifting of peak position,

nor decrease in peak intensity indicating absence of degradation and the second control experiment performed with AgNP in dark (Fig. 7(a)) exhibited decrease in intensity of the peak, though there was no shifting of characteristic peak.

The enhanced photo-catalytic activity in the experiment with AgNPs under UV illumination can be attributed to their large surface area and more active sites on the surface, better light absorption capacity and highly dispersed small particle size without any aggregation. Literature suggests that the morphology, size and crystalline structure of the NP have marked effect on the efficiency of the photo-catalytic activity [39].

3.3.1. Effect of initial dye concentration

The effect of initial dye concentration towards photo-catalytic degradation was investigated considering a range of 1–30 mg/L aqueous CR solution under continuous stirring and UV irradiation. The results indicated that initially the photo-catalytic degradation efficiency increases with increase in the CR concentration (up to 20 mg/L) from 38.77% to 73.83% (Fig. 7(b)). However, photo-degradation efficiency decreased with further increase in the initial concentration of CR beyond the equilibrium concentration (20 mg/L). This might have happened due to two reasons. First, the number of hydroxyl radical ($\cdot\text{OH}$) is constant with a fixed dose of catalyst which got saturated with the dye molecules present in the solution [28] and second, due to hindrance in photo-activation of catalyst as a result of physical adsorption of excessive amount of dye molecules on the surface of the catalysts [40].

3.3.2. Effect of irradiation time

Light plays a key role in the photo-catalytic degradation of dye since the photo-chemical activity is associated with fragmentation and transformation of CR dye into low-molecular-weight by-products as suggested by Ref. [29]. Effect of irradiation time was studied in the range of 15–120 min at earlier optimized initial dye concentration (20 mg/L) under room temperature and UV light irradiation. Residual analysis with a periodic interval of 15 min showed increasing photo-catalytic efficiency with increase in irradiation time up to 73.83% of CR degradation in 90 min (Fig. 7(c)). However, beyond 90 min, there was decrease in degradation efficiency till 120 min. This can be explained by the fact that UV irradiation promotes the valance band to conduction band (CB) which lead to the formation of photoelectron [40,41]. These highly energetic photoelectrons in turn converts the hydroxyl ion (OH^-) into hydroxyl radical ($\cdot\text{OH}$), which are responsible for the photo-chemical degradation of CR [28,41].

3.3.3. Effect of catalyst dose

The catalyst dose is one of the most significant parameter which affects the photo-chemical degradation of dye. Effect of the amount of colloidal AgNPs towards photo-catalytic degradation of CR was studied with a variation of 1:1 to 1:10 ratio of AgNPs and 20 mg/L of CR solution, keeping the previous optimized parameters constant (Fig. 7(d)). It was found that catalytic efficiency increased up to 1:7.5 ratio with a maximum efficiency of 84.79%. But, after the optimum

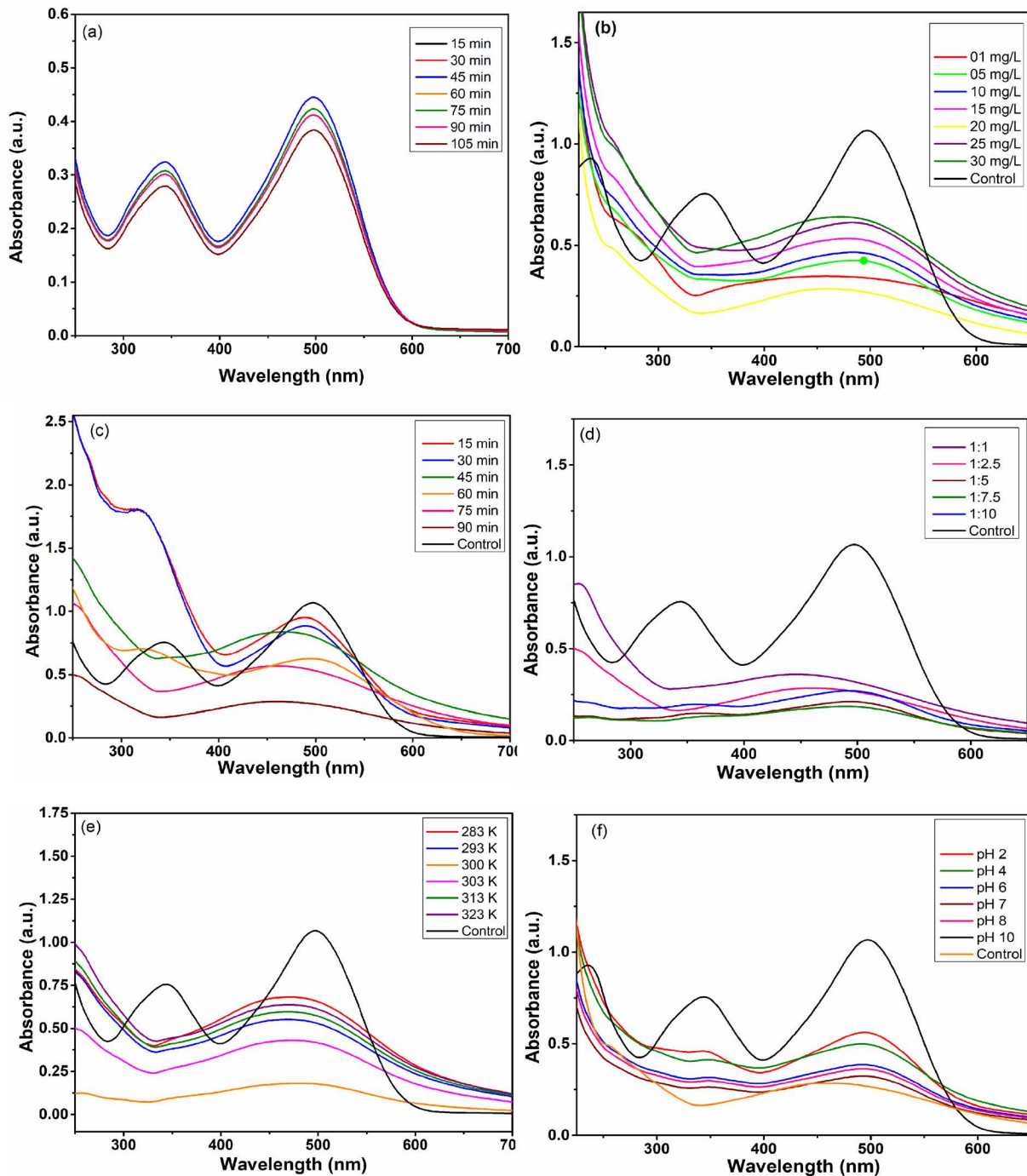


Fig. 7. UV-Visible spectrum of photo-catalytic degradation reaction of CR dye (a) control, (b) effect of initial dye concentration, (c) effect of irradiation time, (d) effect of catalyst dose, (e) effect of temperature and (f) effect of pH.

dose (1:7.5 ratio) the efficiency seemed to dip. Similar result has been reported by Ref. [28] for photo-catalytic degradation of methylene blue using ZnO NPs and methylene blue using AgNPs [42]. Low photo-catalytic efficiency in less dose of catalyst is due to limitation of hydroxyl radical generation in the solution [43]. Nevertheless, if the catalyst dose is beyond the optimum level, then also catalytic efficiency decreases due to inhibition of light penetration dampening the photo-activation process [44].

3.3.4. Effect of temperature

The study on the effect of temperature on photo-catalytic efficiency experimented between 283 and 323 K has shown an incremental trend in degradation efficiency with increasing temperature till the ambient temperature (300 K) (90.02%) and decreased beyond that (Fig. 7(e)). That normally happens due to the photo-selective catalytic reduction activity of the catalyst [45]).

3.3.6. Effect of pH

pH controls the electrochemical properties of a reaction. The photo-catalytic reactions were conducted within a pH range of 2–10 to investigate the effect of pH on the photo-catalytic efficiency (Fig. 7(f)). Maximum efficiency of 90.02% was observed at a neutral pH (pH 7). Generally, the photo-catalytic efficiency of dye is enhanced or inhibited by an electrostatic interaction between surface of the NPs and dye [28]. Beyond the optimum pH the degradation efficiency generally decreases due to changes of the surface charge of the NPs and dye molecule in the solution [46]. The redox potentials of the conduction and valence bands (VBs) also get altered due to change in pH that might affect the photo-catalytic efficiency by restricting interfacial charge transfer [47]. Finally results of all optimization experiments yielded a maximum photo-catalytic degradation of the environmental variables of 90.02%.

3.4. Kinetics study

The photo-catalytic degradation of CR followed pseudo-first-order kinetics and the rate constant (*k*) was calculated from the slope of the logarithmic linear equation using the following formula [48]:

$$\ln\left(\frac{C}{C_0}\right) = -kt \tag{4}$$

where *C*₀ is the initial concentration (mg/L) of CR, *C* is the concentration (mg/L) of CR harvested after every 15 min time interval, *t* is the time (min) and *k* is the rate constant (min⁻¹). The photo-catalytic degradation was validated by the linear relationship between ln(*C/C*₀) and time, indicating good agreement of pseudo-first-order kinetics, model with degradation constant (*k*) = 0.01 min⁻¹ (Fig. 8(a)). The photo-chemical reaction started within 15 min (38.77%) gradually increased with time and reached optimum level at 90 min (90.02%). Result also revealed decrease in *C/C*₀ with respect to time as shown in the Fig. 8(b). Similar results have been reported by Ref. [49].

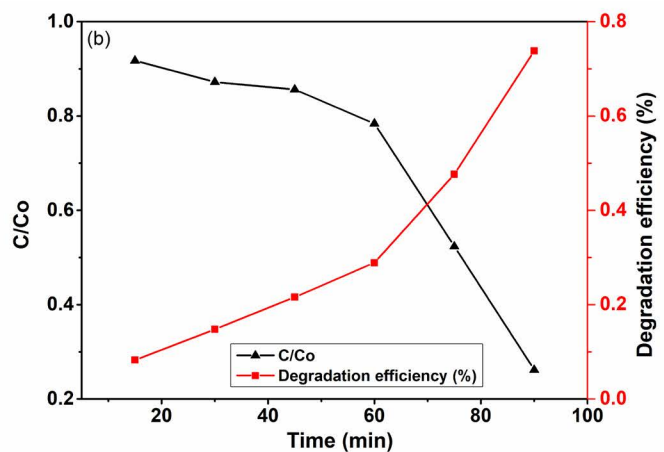
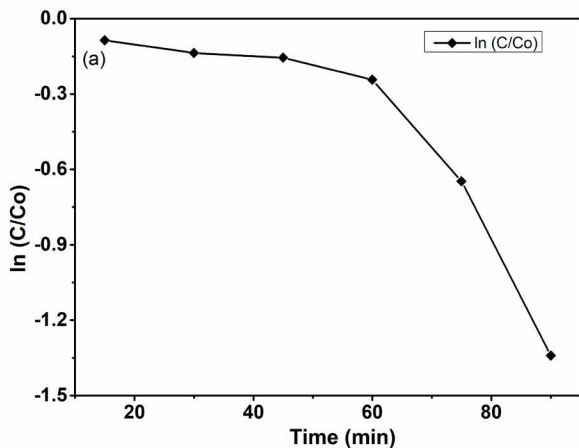


Fig. 8. (a) Kinetic study and (b) time profile of *C/C*₀ and CR degradation efficiency (%).

3.5. Probable mechanism of dye degradation

The photo-catalytic mechanism can be explained by the fact that catalytic reaction occurs only on the surface of the metals due to SPR, and therefore the catalytic efficiency increases with decrease in the particle size up to their critical size [50]. Similar observation on AgNPs was reported by Vidhu and Philip [22], where the authors suggested that large surface area of catalyst (AgNPs) lead to transfer of electrons after the photo-activation in the reactions. In this mechanism the radicals like superoxide radical (O₂⁻), hydroxyl radical (*OH) and hydroperoxyl radical (HO₂^{*}) played an important bridging role in the photo-catalytic degradation process under UV light irradiation [43] (Fig. 9).

The VB electron of the photo-catalyst is promoted to CB electron when the exposed light energy is equivalent or greater than band gap energy, resulting formation of conduction electron (e_{CB}⁻) in the CB and positive hole (h_{VB}⁺) in VB (Eq. (3)) [40]. After formation of the photo-generated species (h_{VB}⁺ and e_{CB}⁻) they are transferred onto the surface of the catalyst (AgNPs), where the h_{VB}⁺ react with water molecule resulting in formation of hydrogen ion (H⁺) and hydroxyl group (OH⁻) (Eq. (4)). Further the OH⁻ group is converted into hydroxyl radical (*OH) by h_{VB}⁺ (Eq. (5)) [51].

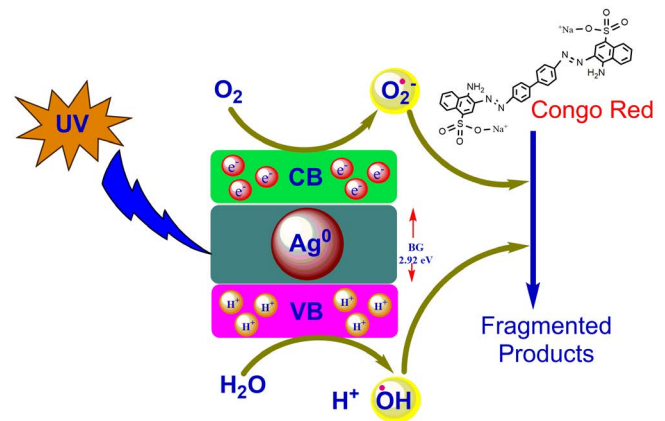
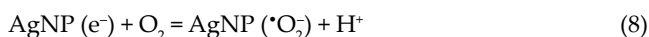
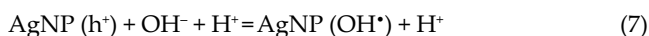


Fig. 9. Proposed mechanism of photo-catalytic degradation of CR using AgNPs.



Fig. 10. Result of germination test of Bengal Gram (*Cicer arietinum*).

On the other hand, e^-_{CB} forms superoxide radical anions ($O_2^{\bullet-}$) by reacting with dissolved oxygen (O_2) on the surface of the catalyst (Eq. (6)) [43]. The $O_2^{\bullet-}$ then react with water molecule and produce hydroperoxyl radical (HO_2^{\bullet}) and $\bullet OH$ (Eq. (7)). Subsequently, these potential $O_2^{\bullet-}$, $\bullet OH$ and HO_2^{\bullet} radicals are oxidizing CR resulting, degraded bi-products and water (H_2O), carbon dioxide (CO_2), nitrate (NO_3^-) and ammonium (NH_4^+) ions. Thus AgNP acts an efficient catalyst in the photo-catalytic reactions.



3.6. Germination test

The germination test performed to determine the toxic effect, if any, on Bengal Gram (*C. arietinum*) seeds showed clear indication of the degraded dye product to be nontoxic (Fig. 10). Germination percentage was 100% in degraded dye product and control, whereas, 60% in 10 and 20 ppm dye. The decrease in germination percentage can be due to the dye induced stress [52]. Apart from this, Seedling Vigour Index was also found to maximum in seeds exposed to degraded dye (169), followed by the seeds in control exposed to double distilled water (121). SVI was 70.8 and 45 in seeds exposed to 10 and 20 ppm, respectively. The maximum SVI of the seeds in degraded product might be due to the presence of additional oxygen, and carbon source after degradation. On the other hand, the set containing the dye solution in different concentrations showed low SVI due to the induced stress [53]

4. Conclusion

Observation of this study suggested that AgNPs biologically synthesized from $AgNO_3$ with neem leaf extract to be having promising degradation capability of toxic dye CR. The

simple extraction procedure of neem leaf by crushing, unlike previous energy intensive boiling process, yielded chemically stable NPs of size range within 35 nm. The NPs formed were crystalline in nature with prominent Ag peaks revealed by EDX and contained functional groups like hydroxyl, alkynes, amide and weak aromatic $-CH$. Grossly the characteristics of the biosynthesized AgNPs exhibited pronounced degradation potential for CR (90%). Further optimization of the environmental process variable of the degradation process indicated optimum condition of room temperature (300 K), pH 7, 20 mg/L initial concentration of CR and a catalyst dose of 1:7.5, finally leading to a significant 90% of degradation within 90 min of reaction. The photo-catalytic degradation process was dominated by pseudo-first-order kinetic model and also suggested that radicals like superoxide ($O_2^{\bullet-}$), hydroxyl ($\bullet OH$) and hydroperoxyl (HO_2^{\bullet}) played a critical role in the photo-catalysis. Degradation of the dye was confirmed through the disappearance of the functional groups of the dye in the FTIR spectra after degradation. Good germination percentage and enhanced Seedling Vigour Index of Bengal Gram (*C. arietinum*) seeds exposed to degraded product also revealed that after degradation the dye was nontoxic. The results of this study can thus be a viable option for remediation of CR.

Acknowledgments

The authors would like to acknowledge the Department of Science and Technology (Government of India), New Delhi for funding the Science & Engineering Research Board, Young Scientist project SR/FTP/ES-2/2013 for undertaking this study. The authors also acknowledge Indian Institute of Technology, Bombay and Central Instrumentation facility of Birla Institute of Technology, Mesra for providing the facility to analyse the silver nanoparticles. The authors also acknowledge Dr Bibhutibhushan Show, Assistant Professor (Dept. of Chemistry, Jadavpur University), who has significantly contributed to the improvement of this manuscript by his substantial inputs and suggestions.

Conflicts of interest

On behalf of all authors, the corresponding author states that there is no conflict of interest.

Symbols and abbreviations

•OH	– Hydroxyl radical
AgNPs	– Silver nanoparticles
CB	– Conduction band
CR	– Congo red
e_{CB}^-	– Conduction electron
h_{VB}^+	– Positive hole
$HO_2^•$	– Hydroperoxyl radical
NPs	– Nanoparticles
$O_2^{•-}$	– Superoxide radical anions
SAED	– Selected area electron diffraction
SPR	– Surface plasmon resonance
SVI	– Seedling vigour index
UV	– Ultraviolet
VB	– Valence band

References

- [1] H.Y. Zhua, R. Jiang, Y.Q. Fu, J.H. Jiang, L. Xiao, G.M. Zeng, Preparation, characterization and dye adsorption properties of $\gamma\text{-Fe}_2\text{O}_3/\text{SiO}_2/\text{chitosan}$ composite, *Appl. Surf. Sci.*, 258 (2011) 1337–1344.
- [2] M. Rafatullah, O. Sulaiman, R. Hashim, A. Ahmad, Adsorption of methylene blue on low-cost adsorbents: a review, *J. Hazard. Mater.*, 177 (2010) 70–80.
- [3] H. Kusic, N. Koprivanac, L. Srsan, Azo dye degradation using Fenton type processes assisted by UV irradiation: a kinetic study, *J. Photochem. Photobiol., A*, 181 (2006) 195–202.
- [4] S.R. Kavitha, M. Umadevi, S.R. Janani, T. Balakrishnan, R. Ramanibai, Fluorescence quenching and photocatalytic degradation of textile dyeing waste water by silver nanoparticles, *Spectrochim. Acta, Part A*, 127 (2014) 115–121.
- [5] T.S. Chandra, S.N. Mudliar, S. Vidyashankar, S. Mukherji, R. Sarada, K. Krishnamurthi, V.S. Chauhan, Defatted algal biomass as a non-conventional low-cost adsorbent: Surface characterization and methylene blue adsorption characteristics, *Bioresour. Technol.*, 184 (2015) 395–404.
- [6] R.V. Khandare, S.P. Govindwar, Phytoremediation of textile dyes and effluents: current scenario and future prospects, *Biotechnol. Adv.*, 33 (2015) 1697–1714.
- [7] M.A. Rauf, S.S. Ashraf, Survey of recent trends in biochemically assisted degradation of dyes, *Chem. Eng. J.*, 209 (2012) 520–530.
- [8] D. Sud, G. Mahajan, M.P. Kaur, Agricultural waste material as potential adsorbent for sequestering heavy metal ions from aqueous solutions – a review, *Bioresour. Technol.*, 99 (2008) 6017–6027.
- [9] D. Sharma, S. Kanchi, K. Bisetty, Biogenic synthesis of nanoparticles: a review, *Arabian J. Chem.* (2015), doi:10.1016/j.arabj.2015.11.002.
- [10] A.K. Mittal, Y. Chisti, U.C. Banerjee, Synthesis of metallic nanoparticles using plant extracts, *Biotechnol. Adv.*, 31 (2013) 346–356.
- [11] Z. Cai, Y. Sun, W. Liu, F. Pan, P. Sun, J. Fu, An overview of nanomaterials applied for removing dyes from wastewater, *Environ. Sci. Pollut. Res.*, 24 (2017) 15882–15904.
- [12] S. Ahmed, M. Ahmad, B.L. Swami, S. Ikram, A review on plants extract mediated synthesis of silver nanoparticles for antimicrobial applications: a green expertise, *J. Adv. Res.*, 7 (2016) 17–28.
- [13] S.F. Kang, C.H. Liao, S.T. Po, Decolourization of textile wastewater by photo-Fenton oxidation technology, *Chemosphere*, 41 (2000) 1287–1294.
- [14] M. Akter, M.T. Sikder, M.M. Rahman, A.K.M.A. Ullah, K.F.B. Hossain, S. Banik, T. Hosokawa, T. Saito, M. Kurasaki, A systematic review on silver nanoparticles-induced cytotoxicity: physicochemical properties and perspectives, *J. Adv. Res.*, 9 (2018) 1–16.
- [15] B. Ajitha, Y.A.K. Reddy, P.S. Reddy, Biogenic nano-scale silver particles by *Tephrosia purpurea* leaf extract and their inborn antimicrobial activity, *Spectrochim. Acta, Part A*, 121 (2014) 164–172.
- [16] P. Pourali, B. Yahyaei, Biological production of silver nanoparticles by soil isolated bacteria and preliminary study of their cytotoxicity and cutaneous wound healing efficiency in rat, *J. Trace Elem. Med. Biol.*, 34 (2016) 22–31.
- [17] K. Vahabi, G.A. Mansoori, S. Karimi, Biosynthesis of silver nanoparticles by fungus *Trichoderma reesei*, *Insciences J.*, 1 (2011) 65–79.
- [18] N.L. Gavade, A.N. Kadam, M.B. Suwarnkar, V.P. Ghodake, K.M. Garadkar, Biogenic synthesis of multi-applicative silver nanoparticles by using *Ziziphus jujuba* leaf extract, *Spectrochim. Acta, Part A*, 136 (2015) 953–960.
- [19] P.D. Shankar, S. Shobana, I. Karuppusamy, A. Pugazhendhi, V.S. Ramkumar, S. Arvindnarayan, G. Kumar, A review on the biosynthesis of metallic nanoparticles (gold and silver) using bio-components of microalgae: formation mechanism and applications, *Enzyme Microb. Technol.*, 95 (2016) 28–44.
- [20] G.G. Selvam, K. Sivakumar, Phycosynthesis of silver nanoparticles and photocatalytic degradation of methyl orange dye using silver (Ag) nanoparticles synthesized from *Hypnea musciformis* (Wulfen) J.V. Lamouroux, *Appl. Nanosci.*, 5 (2015) 617–622.
- [21] K. Roy, C.K. Sarkar, C.K. Ghosh, Photocatalytic activity of biogenic silver nanoparticles synthesized using yeast (*Saccharomyces cerevisiae*) extract, *Appl. Nanosci.*, 5 (2015) 953–959.
- [22] V.K. Vidhu, D. Philip, Catalytic degradation of organic dyes using biosynthesized silver nanoparticles, *Micron*, 56 (2014) 54–62.
- [23] F. Baghbani-Arani, R. Movagharnia, A. Sharifian, S. Salehi, S.A.S. Shandiz, Photo-catalytic, anti-bacterial, and anti-cancer properties of phyto-mediated synthesis of silver nanoparticles from *Artemisia tournefortiana* Rchb extract, *J. Photochem. Photobiol., B*, 173 (2017) 640–649.
- [24] P. Frid, S.V. Anisimov, N. Popovic, Congo red and protein aggregation in neurodegenerative diseases, *Brain Res. Rev.*, 53 (2007) 135–160.
- [25] A. Mittal, J. Mittal, A. Malviya, V.K. Gupta, Adsorptive removal of hazardous anionic dye “Congo red” from wastewater using waste materials and recovery by desorption, *J. Colloid Interface Sci.*, 340 (2009) 16–26.
- [26] K. Girish, S.S. Bhat, Neem – a green treasure, *Electron. J. Biol.*, 4 (2008) 102–111.
- [27] S. Ahmed, Saifullah, M. Ahmad, B.L. Swami, S. Ikram, Green synthesis of silver nanoparticles using *Azadirachta indica* aqueous leaf extract, *J. Radiat. Res. Appl. Sci.*, 9 (2016) 1–7.
- [28] G. Bandekar, N.S. Rajurkar, I.S. Mulla, U.P. Mulik, D.P. Amalnerkar, P.V. Adhyapak, Synthesis, characterization and photocatalytic activity of PVP stabilized ZnO and modified ZnO nanostructures, *Appl. Nanosci.*, 4 (2014) 199–208.
- [29] I. Bibi, N. Nazar, M. Iqbal, S. Kamal, H. Nawaz, S. Nouren, Y. Safa, K. Jilani, M. Sultan, S. Ata, F. Rehman, M. Abbas, Green and eco-friendly synthesis of cobalt-oxide nanoparticle: characterization and photo-catalytic activity, *Adv. Powder Technol.*, 28 (2017) 2035–2043.
- [30] B. Ajitha, Y.A.K. Reddy, P.S. Reddy, Green synthesis and characterization of silver nanoparticles using *Lantana camara* leaf extract, *Mater. Sci. Eng., C*, 49 (2015) 373–381.
- [31] M.A. Farah, M.A. Ali, S. Chen, Y. Li, F.M. Al-Hemaid, F.M. Abou-Tarboush, K.M. Al-Anazi, J. Lee, Silver nanoparticles synthesized from *Adenium obesum* leaf extract induced DNA damage, apoptosis and autophagy via generation of reactive oxygen species, *Colloids Surf., B*, 141 (2016) 158–169.
- [32] B. Ajitha, Y.A.K. Reddy, K.M. Rajesh, P.S. Reddy, *Sesbania grandiflora* leaf extract assisted green synthesis of silver nanoparticles: antimicrobial activity, *Mater. Today*, 3 (2016) 1977–1984.
- [33] V. Dhand, L. Soumya, S. Bharadwaj, S. Chakra, D. Bhatt, B. Sreedhar, Green synthesis of silver nanoparticles using *Coffea arabica* seed extract and its antibacterial activity, *Mater. Sci. Eng., C*, 58 (2016) 36–43.
- [34] O. Azizian-Shermeh, A. Einali, A. Ghasemi, Rapid biologically one-step synthesis of stable bioactive silver nanoparticles

- using Osage orange (*Maclura pomifera*) leaf extract and their antimicrobial activities, *Adv. Powder Technol.* 28, (2017) 3164–3171.
- [35] B. Sadeghi, F. Gholamhoseinpoor, A study on the stability and green synthesis of silver nanoparticles using *Ziziphora tenuior* (Zt) extract at room temperature, *Spectrochim. Acta, Part A*, 134 (2015) 310–315.
- [36] P.S. Ramesh, T. Kokila, D. Geetha, Plant mediated green synthesis and antibacterial activity of silver nanoparticles using *Embllica officinalis* fruit extract, *Spectrochim. Acta, Part A*, 142 (2015) 339–343.
- [37] G.C.J. Swarnavalli, S. Dinakaran, N. Raman, R. Jegadeesh, C. Pereira Bio inspired synthesis of monodispersed silver nano particles using *Sapindus emarginatus* pericarp extract – study of antibacterial efficacy, *J. Saudi Chem. Soc.*, 21 (2017) 172–179.
- [38] K. Tahir, S. Nazir, B. Li, A.U. Khan, Z.U.H. Khan, A. Ahmad, F.U. Khan, An efficient photo catalytic activity of green synthesized silver nanoparticles using *Salvadora persica* stem extract, *Sep. Purif. Technol.*, 150 (2015) 316–324.
- [39] Z.U.H. Khan, A. Khan, A. Shah, Y. Chen, P. Wan, A.U. Khan, K. Tahir, N. Muhamma, F.U. Khan, H.U. Shah, Photocatalytic, antimicrobial activities of biogenic silver nanoparticles and electrochemical degradation of water soluble dyes at glassy carbon/silver modified past electrode using buffer solution, *J. Photochem. Photobiol., B*, 156 (2016) 100–107.
- [40] R. Karthik, M. Govindasamy, S. Chen, Y. Cheng, P. Muthukrishnan, S. Padmavathy, A. Elangovan, Biosynthesis of silver nanoparticles by using *Camellia japonica* leaf extract for the electrocatalytic reduction of nitrobenzene and photocatalytic degradation of Eosin-Y, *J. Photochem. Photobiol., B*, 170 (2017) 164–172.
- [41] K. Tahir, A. Ahmad, B. Li, S. Nazir, A.U. Khan, T. Nasir, Z.U.H. Khan, R. Naz, M. Raza, Visible light photo catalytic inactivation of bacteria and photo degradation of methylene blue with Ag/TiO₂ nanocomposite prepared by a novel method, *J. Photochem. Photobiol., B*, 162 (2016) 189–198.
- [42] E.S. Aazam, Photocatalytic degradation of Congo red under visible light irradiation using Pd-Bi_{3.84}W_{0.16}O_{6.24} nanocomposite, *J. Alloys. Compd.*, 644 (2015) 1–6.
- [43] K. Saravanakumar, V. Muthuraj, S. Vadivel, Constructing novel Ag nanoparticles anchored on MnO₂ nanowires as an efficient visible light driven photocatalyst, *RSC Adv.*, 6 (2016) 61357–61366.
- [44] C.B. Ong, A.W. Mohammad, R. Rohani, M.M. Ba-Abbad, N.H.H. Hairom, Solar photocatalytic degradation of hazardous Congo red using low-temperature synthesis of zinc oxide nanoparticles, *Process Saf. Environ. Prot.*, 104 (2016) 549–557.
- [45] A. Yamamoto, Y. Mizuno, K. Teramura, T. Shishido, T. Tanaka, Effects of reaction temperature on the photocatalytic activity of photo-SCR of NO with NH₃ over a TiO₂ Photocatalyst, *Catal. Sci. Technol.*, 3 (2013) 1771–1775.
- [46] J.Z. Kong, A.D. Li, X.Y. Li, H.F. Zhai, W.Q. Zhang, Y.P. Gong, H. Li, D. Wu, Photodegradation of methylene blue using Ta-doped ZnO nanoparticle, *J. Solid State Chem.*, 183 (2010) 1359–1364.
- [47] Y.H. Jiang, Y.M. Sun, H. Liu, F.H. Zhu, H.B. Yin, Solar photocatalytic decolorization of C.I. Basic blue 41 in an aqueous suspension of TiO₂-ZnO, *Dyes Pigm.*, 78 (2008) 77–83.
- [48] E. Haritha, S.M. Roopan, G. Madhavi, G. Elango, N.A. Al-Dhabi, M.V. Arasu, Green chemical approach towards the synthesis of SnO₂ NPs in argument with photocatalytic degradation of diazo dye and its kinetic studies, *J. Photochem. Photobiol., B*, 162 (2016) 441–447.
- [49] M.D. Murcia, M.M. Gómez, E. Gómez, J.L. Gómez, N. Christofi, Photodegradation of congo red using XeBr, KrCl and Cl₂ barrier discharge excilamps: a kinetics study, *Desalination*, 281 (2011) 364–371.
- [50] H. Li, Z. Li, Y. Yu, Y. Ma, W. Yang, F. Wang, X. Yin, X. Wang, Surface-plasmon-resonance-enhanced photoelectrochemical water splitting from Au-nanoparticle-decorated 3D TiO₂ nanorod architectures, *J. Phys. Chem. C*, 121 (2017) 12071–12079.
- [51] M. Thomas, G.A. Naikoo, M.U.D. Sheikh, M. Bano, F. Khan, Effective photocatalytic degradation of Congo red dye using alginate/carboxymethyl cellulose/TiO₂ nanocomposite hydrogel under direct sunlight irradiation, *J. Photochem. Photobiol., A*, 327 (2016) 33–43.
- [52] K. Babu, G. Rosaiah, A study on germination and seedling growth of Blcakgram (*Vigna mungo* L. Hepper) germplasm against Polyethylene glycol 6000 stress, *IOSR J. Pharm. Biol. Sci.*, 5 (2017) 90–98.
- [53] G.U.G. Ping, W.U.G. Rong, L.C. Mei, Z.C. Fang, Effects of PEG priming on vigor index and activated oxygen metabolism in soybean seedlings, *Chinese J. Oil Crop. Sci.*, 22 (2000) 26–30.